Application of a Multiple Mapping Conditioning Mixing Model to ECN Spray A

Achinta Varna[a,*], Armin Wehrfritz[a], Evatt. R. Hawkes[a,b], Matthew. J. Cleary[c], Tommaso Lucchini[d], Gianluca D'Errico[d], Sanghoon Kook[a], Qing. N. Chan[a]

[a] *School of Mechanical and Manufacturing Engineering,University of New South Wales, Sydney, NSW 2052, Australia*
[b] *School of Photovoltaic and Renewable Energy Engineering,University of New South Wales, Sydney, NSW 2052, Australia*
[c] *School of Aerospace, Mechanical and Mechatronic Engineering,University of Sydney, Sydney, NSW 2006, Australia*
[d] *Department of Energy, Politecnico di Milano, Milan, 20156, Italy*

Abstract

The engine combustion network (ECN) Spray A is modelled using the Reynolds-averaged Navier–Stokes-transported probability density function (RANS-TPDF) approach to validate the application of a new multiple mapping conditioning (MMC) mixing model to multiphase reactive flows. The composition TPDF equations are solved using a Lagrangian stochastic approach and the spray is modelled with a discrete particle approach. The model is first validated under non-reacting conditions (at 900 K) using experimental mixture-fraction data. Reactive simulations are then performed for three different ambient temperatures (800, 900, 1100 K) and oxygen concentrations (13, 15, 21%) at an ambient density of 22.8 $\mathrm{kg/m^3}$. The MMC mixing model is compared with the interaction by exchange with the mean (IEM) mixing model. The ignition delay predictions are not sensitive to the mixing model and are predicted well by both the mixing models under all the tested ambient conditions. The IEM model overpredicts the flame lift-off length (FLOL) at high temperature and high oxygen conditions with a mixing constant $C_\phi = 2$. The MMC model with $C_\phi = 2$ and a target correlation coefficient $r_t = 0.935$ between the mixture fraction and a reference variable used to condition mixing predicts good FLOL under all the conditions except 800 K. It is demonstrated that the lift-off length is controllable by changing the target correlation coefficient, while C_ϕ and therefore the mixing fields are held fixed. In comparison to the MMC model, the IEM model predicts a higher variance of temperature conditioned on mixture fraction near the flame base owing to its lacking the property of localness. The mixing distance between the notional TPDF particles in the composition space is also higher with the IEM model and it is demonstrated that by changing r_t, different levels of mixing locality can be achieved.

Keywords:
MMC, TPDF, mixing model, ECN, combustion

*Corresponding author
Email address: a.varna@unsw.edu.au (Achinta Varna)

1. Introduction

Diesel engines play an important role in the heavy-duty transport and power generation sectors, and this is likely to remain the case for the foreseeable future, due to their high power density and efficiency. However, reducing emissions of particulate matter, nitrogen oxides and CO_2, and improving fuel economy in order to reduce the impact on the environment and human health constitute major challenges.

The design and optimisation of improved engines that can address the above-mentioned challenges would be facilitated by the availability of accurate, validated computational models. One key issue these models need to handle is that turbulent fluctuations of the thermochemical state can be significant and cannot be directly resolved with computationally affordable meshes – leading to a problem often referred to as turbulence-chemistry interactions (TCI). Numerous computational fluid dynamic (CFD) studies, employing various combustion models [1–3], have been conducted in the context of atmospheric flames which furthered the understanding of TCI. However, TCI under diesel engine conditions has received less attention. Historically, this was in part due to the lack of sufficiently detailed and well-characterised experimental measurements which were suitable for examining TCI effects in models. To rectify this gap, and to facilitate the exchange between experimental and numerical engine research, an international research collaboration, the Engine Combustion Network (ECN), has been established. Various target conditions for diesel spray combustion have been defined and investigated within the ECN. A wide range of combustion models has been applied to the ECN sprays, including perfectly stirred reactor (PSR) models [4], flamelet models [5], conditional moment closure (CMC) [6] and transported probability density function (TPDF) methods [7–9].

The TPDF method [10] is a promising technique for diesel combustion since it can, in principle, model multiple combustion modes (i.e. premixed, nonpremixed and partially-premixed) and can capture processes on a wide range of time scales. The fact that the chemical source term appears in closed form is also presumably an advantage in chemistry-driven processes such as ignition and pollutant formation. However, TPDF methods require a mixing model to approximate the molecular transport in composition space. A list of ideal properties of a mixing model can be found in [11]. It has been reported that the localness property, i.e. the property that change of composition due to mixing is influenced by the neighbourhood in composition space, is important. A mixing model should also be able to predict the correct scalar variance (or unconditional fluctuations) decay rate. However, Klimenko [12] suggested that the conditional fluctuations, i.e. fluctuations of a scalar around the mean conditioned on another scalar (e.g. mixture fraction), should also be predicted accurately by a mixing model to capture high TCI. The mixing models employed in most of the TPDF studies of ECN Spray A [7, 8] were either the interaction by exchange with the mean (IEM) [13], the modified Curl's (MC) [14] or the Euclidean minimum spanning tree (EMST) [11]. The IEM and the MC models do not have the localness property [11] and the EMST model has been shown in many circumstances to under-predict conditional fluctuations [15]. Multiple mapping conditioning (MMC) [16] provides a method to control the dissipation rate of the unconditional and the conditional fluctuations independently by distinguishing between the major variables, i.e. the variables which are allowed to fluctuate independently, and the minor variables, i.e. the variables which fluctuate only jointly with the major variables. In most of the MMC studies, a single reference variable (based on mixture fraction for non-premixed and partially-premixed flames) is used as a major variable, where the species mass fractions and specific enthalpy are the minor variables. The MMC model has been applied to Spray A in the context of sparse-Lagrangian large-eddy simulation [9].

Recently, we proposed a new MMC mixing model [17] and applied this successfully to a non-premixed methane-air flame series (Sandia D-F) [18]. In the current work, we extend this model to diesel spray combustion, and apply it to Spray A in the context of a Reynolds-averaged Navier–Stokes (RANS)-TPDF approach. First, non-reactive simulations are validated using experimental mixture-fraction data and the reactive calculations are subsequently verified using the ignition delay time and flame lift-off length. The performance of the local MMC model and the non-local IEM model are analysed quantitatively.

2. The MMC mixing model

The evolution of a one-time, one-point Eulerian composition TPDF is given by [19]

$$\begin{aligned}\frac{\partial \rho f_\phi}{\partial t} + \frac{\partial \rho \widetilde{u_i} f_\phi}{\partial x_i} + \frac{\partial \omega_k f_\phi}{\partial \psi_k} &= -\frac{\partial}{\partial x_i}\left[\langle u_i' | \boldsymbol{\psi}\rangle \rho f_\phi\right] \\ &+ \frac{\partial}{\partial \psi_k}\left[\left\langle \frac{\partial J_i^k}{\partial x_i}\middle|\boldsymbol{\psi}\right\rangle f_\phi\right] + \left\langle \rho^{-1} S_m | \boldsymbol{\psi}\right\rangle \rho f_\phi \\ &- \frac{\partial}{\partial \psi_k}\left[\left\langle \rho^{-1} S_\phi - \phi_k \rho^{-1} S_m | \boldsymbol{\psi}\right\rangle \rho f_\phi\right],\end{aligned} \tag{1}$$

where f_ϕ is the TPDF of the composition vector ϕ_k, which includes chemical species mass fractions and mixture specific enthalpy. The density, Favre mean velocity, chemical source term, spray source term for the composition vector and spray source term for mass are represented by ρ, $\widetilde{u_i}$, ω_k, S_ϕ and S_m, respectively. The symbols J_i^k and ψ_k denote the molecular flux and the sample space of ϕ_k, respectively. The tilde, single prime and $\langle|\rangle$ notations indicate unconditional Favre average, unconditional Favre fluctuation and conditional Reynolds average, respectively. The first two terms on the right hand side of Eq. (1) represent the turbulent transport in physical space and the molecular transport in composition space, respectively. The gradient transport hypothesis is used for the closure of the former and a mixing model is used for the latter [10]. The last two terms are due to spray evaporation and are closed using a simple model in which the mass and enthalpy spray source terms are distributed to notional particles in proportion to their mass [20].

The TPDF equation can be recast into a computationally efficient, stochastic Lagrangian form, which yields the following equations for the evolution of notional particles [19]:

$$dx_i^* = \left(\widetilde{u_i} + \frac{1}{\overline{\rho}}\frac{\partial \Gamma_{\text{eff}}}{\partial x_i}\right)dt + \left(\frac{2\Gamma_{\text{eff}}}{\overline{\rho}}\right)^{\frac{1}{2}} dW_i, \tag{2}$$

$$dm^* = m_s \frac{m^*}{\Sigma_{*=1}^{n_p} m^*}, \tag{3}$$

$$d\phi_k^* = d\phi_{k,\omega}^* + d\phi_{k,s}^* + d\phi_{k,mix}^* \,, \tag{4}$$

where *, $W_i(t)$, m_s and n_p represent notional particle properties, an independent Wiener process, evaporated mass from spray and the number of notional particles per cell, respectively. The effective diffusivity, Γ_{eff} , is calculated as

$$\Gamma_{\text{eff}} = \mu/\sigma_\phi + \mu_T/\sigma_{T\phi}, \tag{5}$$

where μ, μ_T, σ_ϕ and $\sigma_{T\phi}$ denote molecular and turbulent dynamic viscosities, and molecular and turbulent Schmidt numbers, respectively.

Equation (4) represents the transport of TPDF particles in the composition space where the terms $d\phi_{k,\omega}^*$ and $d\phi_{k,s}^*$ denote the change in composition due to chemical reactions and spray evaporation, respectively. The molecular transport in composition space ($d\phi_{k,mix}^*$) is closed using a mixing model, where the IEM [13] and a recently developed MMC mixing model [17] are evaluated in the present study. For the IEM model the mixing term is given by

$$d\phi_{k,mix}^* = -\frac{C_\phi}{2\tau}(\phi_k^* - \widetilde{\phi_k})dt, \tag{6}$$

where C_ϕ is the mixing model constant and τ is the turbulence timescale, which is computed from the turbulent kinetic energy, k, and its dissipation rate, ε, as $\tau = k/\varepsilon$. The MMC mixing model equations [18], extended for the case of an evaporating spray, are

$$d\xi^* = d\xi_s^* + d\xi_{mix}^* \,, \tag{7}$$

$$d\xi_{mix}^* = -\frac{C_\phi}{\tau}(\xi^* - \widetilde{\xi})dt + b_o\left(\frac{2C_\phi\widetilde{\xi''^2}}{\tau}\right)^{\frac{1}{2}} dW_\xi \,, \tag{8}$$

$$d\phi_{k,mix}^* = -\frac{C_\phi}{2(1-r_t^2)\tau}(\phi_k^* - \widetilde{\phi_k|\xi})dt \,, \tag{9}$$

where ξ is the reference variable, W_ξ is another independent Wiener process and $\widetilde{\phi_k|\xi}$ is the Favre mean of ϕ_k conditioned on ξ. The reference variable has statistics similar to that of the mixture fraction (Z): $\widetilde{\xi} \approx \widetilde{Z}$, $\widetilde{\xi''^2} \approx \widetilde{Z''^2}$. The change in reference variable due to droplet evaporation, $d\xi_s^*$, is equal to the change in mixture fraction due to droplet evaporation. The model constant b_o takes a fixed value of 0.71 to ensure $\widetilde{\xi''^2} \approx \widetilde{Z''^2}$ [21], and the constants C_ϕ and r_t control the dissipation rate of unconditional and conditional fluctuations, respectively [17]. The reference variable in the current MMC mixing model is different from that of the original formulation by Klimenko and Pope [16]. These differences have been analysed in our previous work on ideal flow cases and the Sandia flame series [17, 18]. The MMC model is by definition local in ξ-space but the mixing is expected to be local in Z-space for nonpremixed and partially-premixed combustion. The target correlation coefficient, r_t, determines the level of correlation between Z and ξ, and hence the degree of localness in Z. The details of the mixing model implementation can be found in [18]. In this study, the standard value of $C_\phi = 2$ [22] is used for both the IEM and the MMC model. Wandel and Klimenko [23] suggest that the ratio of the dissipation timescale for unconditional fluctuations to the dissipation timescale for conditional fluctuations takes a nominal value of eight which corresponds to $r_t = 0.935$ and has been found to work well for Sandia flames D-F by Varna et al. [18]. The same value will be tested for Spray A in this study and a significantly lower value of $r_t = 0.5$ is also tested to examine the sensitivity of the predictions.

It is desirable for mixing to be local in composition space but to satisfy the independence and linearity principles [11] the mixing model is local in a reference variable space that is correlated to the composition through the mixture fraction. The level of localness in composition space is therefore enforced indirectly and can be

quantified through the mixing distance defined as

$$d_{mix} = \left(\frac{1}{n_p} \Sigma_{*=1}^{n_p} \Sigma_{k=1}^{n_\alpha} (Y_k^* - \widehat{Y_k})^2 \right)^{\frac{1}{2}}, \quad (10)$$

where n_α is the number of chemical species, Y_k^* is the mass fraction of species k and $\widehat{Y_k}$ is an average term of species k. In the IEM model, $\widehat{Y_k} = \widetilde{Y_k}$ and in the MMC model $\widehat{Y_k} = \widetilde{Y_k|\xi}$, which can be inferred from Eqs. (6) and (9), respectively.

3. Experimental data

The experimental test case for validation of the computational results is ECN Spray A. The experimental set-up consists of a constant volume combustion chamber for which different ambient conditions are achieved by a pre-burn event. The experiments were carried out at Sandia National Laboratories [24, 25] and the data is available on the ECN web-pages [26]. The liquid *n*-dodecane fuel is injected from a single-hole, high-pressure injector. A summary of the ambient conditions and injector data used in the present study is given in Table 1.

Table 1: Experimental conditions

Parameter	Value
Ambient Temperature	800, 900, 1100 K
Ambient Density	22.8 kg/m^3
Ambient Oxygen	0, 13, 15, 21% by volume
Nozzle Diameter	0.09 mm
Fuel Temperature	363 K
Injection Pressure	150 MPa
Injection Duration	6 ms

The experimental validation data for the non-reacting case includes the liquid length, the vapour penetration and the mixture-fraction field, and for the reactive cases the ignition delay time and lift-off length. Detailed information regarding the experimental set-up and measurement techniques can be found in Ref. [24, 25].

4. Numerical methods

The numerical simulations are carried out using a two-way coupled RANS-TPDF solver implemented in OpenFOAM-2.4.x [27]. The continuous gas phase velocity, pressure and turbulence quantities (k, ε and μ_T) are obtained from a finite-volume (FV) solver and passed to the Lagrangian solver for the notional particles. The TPDF solver evolves the notional particles and computes the species mass fractions and absolute enthalpy which are passed back to the FV solver where the density is obtained using the equivalent enthalpy method [28]. A particle control algorithm [9] is used to ensure uniform distribution of statistical error by maintaining approximately the same number of notional TPDF particles in each FV cell. A detailed description of the TPDF algorithm is given in Ref. [9, 18].

A standard discrete-particle method is employed to model the liquid fuel spray [29]. The droplet evaporation is estimated using the D^2-law and the appropriate relaxation times calculated under standard evaporation conditions. The droplet mass (m_d) and temperature (T_d) equations are [30]

$$\frac{dm_d}{dt} = -\frac{m_d}{\tau_e}, \quad (11)$$

$$\frac{dT_d}{dt} = \frac{\widetilde{T} - T_d}{\tau_h} f - \frac{h_v}{c_{l,d}\tau_e}, \quad (12)$$

where $\widetilde{T}$ is the Favre-averaged gas temperature, τ_e is the relaxation time under standard evaporation conditions, τ_h is the heat transfer relaxation time, h_v is the vaporisation enthalpy, $c_{l,d}$ is the specific heat of liquid and the factor f accounts for heat transfer associated with evaporation. The time scales of evaporation (τ_e) and heat transfer (τ_h) are [30]

$$\tau_e = \frac{m_d}{\pi D \rho_v \ln\left(\frac{1-X_{v,\infty}}{1-X_{v,s}}\right)} \frac{1}{Sh} \frac{\bar{\rho}\sigma}{\mu}, \quad (13)$$

$$\tau_h = \frac{m_d c_{l,d}}{\pi D \kappa Nu}, \quad (14)$$

where ρ_v is the density of fuel vapour close to the droplet surface, Sh is the Sherwood number, Nu is the Nusselt number, κ is the thermal conductivity, $X_{v,s}$ is the equilibrium vapour mole fraction of the evaporating component at the droplet surface and $X_{v,\infty}$ is the mole fraction of the evaporating component in the gas phase. The thermodynamic conditions in the present work are such that boiling does not occur. Eqs. (11) and (12) provide spray source terms for mass and enthalpy which are distributed to the notional particles (cf. Eqs. (3) and (4)). Droplet breakup is accounted for using the Kelvin-Helmholtz Rayleigh-Taylor (KHRT) model [31] and turbulent dispersion of droplets is modelled by a stochastic model. The number of parcels injected per second is 50000 and all injected parcels have the same droplet diameter. Further details regarding the spray submodels can be found in Ref. [29, 32].

Table 2: Numerical set-up

Model	Value
Domain	108 mm x 60 mm
Time-step	0.5 μs
Discretization	1^{st} order in time
	2^{nd} order in space
Chem. mechanism	Yao et al. [33] (54 species)
Schmidt numbers	$\sigma_\phi = 0.7$, $\sigma_{T\phi} = 0.7$
TPDF particles/cell	200
Mixing model	MMC: $C_\phi = 2$; $r_t = 0.5, 0.935$
	IEM: $C_\phi = 2$
Turbulence model	Standard k-ε [34]: $C_{\varepsilon 1} = 1.57$,
	$C_{\varepsilon 2} = 1.92$, $C_\mu = 0.09$
Secondary breakup	KHRT: $B_1 = 15$, $C_{RT} = 0.5$

The details of the numerical set-up are given in Table 2. The computational domain consists of a 2D axisymmetric, non-uniform mesh with an axial length of 108 mm and a radial length of 60 mm, representing the same volume as that of the combustion chamber in the experiments. The mesh has 7040 cells refined towards the centreline and the nozzle, where the size of the smallest cell is 0.4 mm x 0.2 mm. No-slip and adiabatic boundary conditions are applied at the walls of the combustion chamber and the TPDF particles are reflected from the solid walls. Uniform initial conditions are applied for density, temperature and species mass fraction and the ambient gas composition corresponds to that of the Sandia pre-burn chamber [35]. The initial gas velocity is assumed to be zero, the initial turbulent kinetic energy is $k_0 = 0.735\,\mathrm{m}^2/\mathrm{s}^2$ [7] and the initial turbulence dissipation rate is $\varepsilon_0 = 5.67\,\mathrm{m}^2/\mathrm{s}^3$ based on the turbulence integral length scale of 0.01 mm. The chemical mechanism is a 54 species, 269 reactions reduced mechanism [33], which has been employed in a number of other studies of Spray A [36].

5. Results and discussion

5.1. Non-reacting case

As a first step in the validation of the spray combustion simulations of the ECN Spray A cases, the flow field under non-reacting conditions is compared with the experimental data to ensure that the mesh, spray sub-models, turbulence model and the implementation of conservations laws are accurate. In our preliminary work on non-reacting Spray A [37] a consistent evolution of the gas phase mass in the FV and TPDF solvers was shown for cases with source terms due to liquid fuel evaporation, thus demonstrating a consistent implementation with respect to mass conservation. Further, a good agreement between the simulated and experimental liquid length and vapour penetration was shown (see supplementary material), demonstrating that the turbulence and spray sub-models are capturing the spray dynamics well.

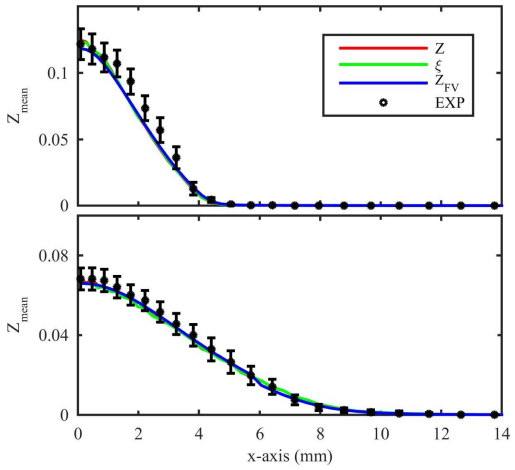

Figure 1: Radial mixture fraction mean profiles at $z = 25$ mm (top) and $z = 45$ mm (bottom).

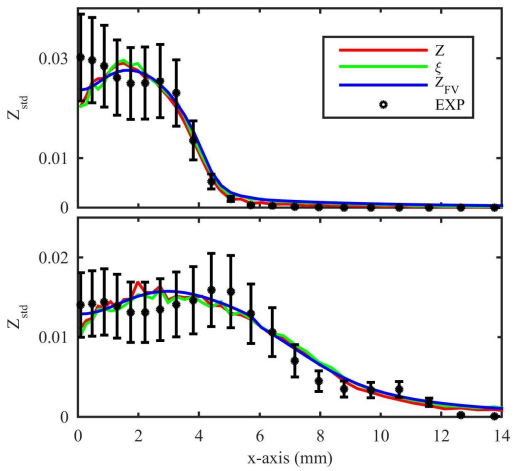

Figure 2: Radial mixture fraction standard deviation profiles at $z = 25$ mm (top) and $z = 45$ mm (bottom).

Figures 1 and 2 show a comparison of the mean and the standard deviation for the mixture fraction (red line) and the reference variable (green line) obtained from the TPDF particles, and experimental measurements (symbols). Also shown are the mean and standard deviation values for mixture fraction obtained from the respective transport equations in the FV solver (blue line) [38].

The good agreement between Z_{std} from the TPDF and FV solver indicates that there is no significant bias error in the TPDF solver. The excellent agreement between the Z_{mean} and Z_{std} of TPDF solver and the experimental data further validates the choices for the main parameters that influence these quantities: $C_\phi = 2$, $\sigma_{T\phi} = 0.7$ and $C_{\varepsilon 1} = 1.57$ ($C_{\varepsilon 1}$ was modified to account for round jet anomaly [8]). It can also be observed that $\widetilde{\xi} \approx \widetilde{Z}$ and $\widetilde{\xi''^2} \approx \widetilde{Z''^2}$ according to the requirements of the MMC mixing model [17].

5.2. Reacting cases

This section presents the results of reacting cases with three different ambient temperatures (T_{amb}) and three different oxygen concentrations ($O_{2,amb}$) as shown in Table 1. Experimental data is available for the ignition delay (ID) and flame lift-off length (FLOL). In simulations, the ID is defined as the time difference between the start of injection and the maximum rate of rise of the maximum Favre-averaged temperature as suggested by previous works [8]. The FLOL is defined as the minimum distance between the nozzle and the location where the OH mass fraction (Y_{OH}) reaches 15% of the maximum value in the combustion chamber at a given ambient condition [39].

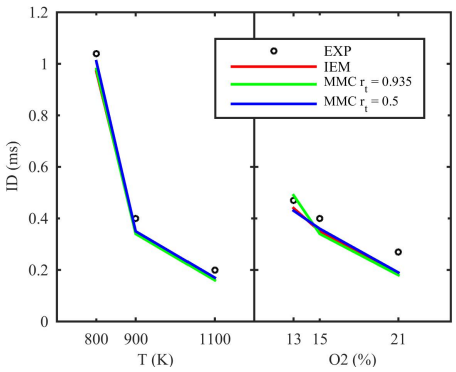

Figure 3: Comparison of ignition delay predictions of experiments, and IEM and MMC mixing models at different ambient conditions.

Figure 3 shows that the ID is predicted well by all mixing models under different ambient conditions. The trend of decrease in ID with increase in ambient temperature and oxygen concentration is captured accurately. There is a negligible effect of the choice of mixing model (IEM or MMC) or of r_t on ID predictions, which is in line with previous observations with other models [8].

Figure 4 shows the effect of different mixing models on the FLOL predictions. The IEM mixing model with

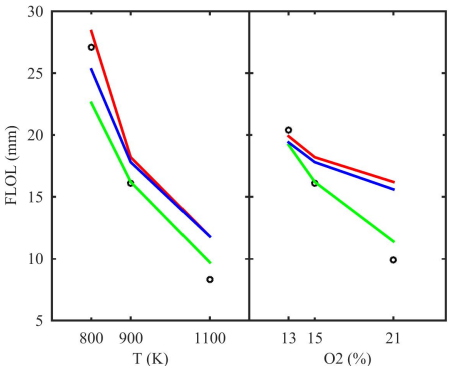

Figure 4: Comparison of lift-off length predictions of experiments, and IEM and MMC mixing models at different ambient conditions.

$C_\phi = 2$ overpredicts the FLOL for the conditions with a higher reactivity ($T_{\text{amb}} = 900$ K and $T_{\text{amb}} = 1100$ K, and 15% and 21% $O_{2,\text{amb}}$). A common practice is to vary C_ϕ in order to improve the FLOL predictions under different ambient conditions [8, 40]. However, this would affect the distribution of $\widetilde{Z''^2}$ and one has to go back to the non-reactive case to tune the turbulence model to get correct predictions of $\widetilde{Z''^2}$. In spite of the modifications it might not be possible to get accurate FLOL predictions for different ambient conditions with a single value of C_ϕ. On the other hand, the MMC mixing model controls the dissipation of unconditional and conditional fluctuations independently using C_ϕ and r_t, respectively. Hence, the MMC mixing model is able to predict the FLOL accurately under different ambient conditions with the same mixture-fraction field (same C_ϕ value) by controlling the dissipation rate of the conditional fluctuations of reactive scalars (varying r_t).

Figure 4 shows that the MMC model predicts the FLOL well for different $O_{2,\text{amb}}$ conditions with $r_t = 0.935$. The FLOL is also predicted well at 900 K and 1100 K whereas a significant under-prediction is observed for the 800 K case. It is shown in Fig. 4 that decreasing the value of r_t to 0.5 increases the FLOL under all ambient conditions since a lower r_t value results in a lower dissipation rate of conditional fluctuations of reactive scalars. Further, the MMC model with a low r_t value has predictions similar to that of the IEM model since the IEM model does not have the localness property and the MMC model with low r_t implies less localness. The results therefore demonstrate that FLOL predictions can be controlled by changing r_t and thus the level of locality provided by the model. Further work and experience across a wider range of conditions will be needed to recommend optimal values for r_t.

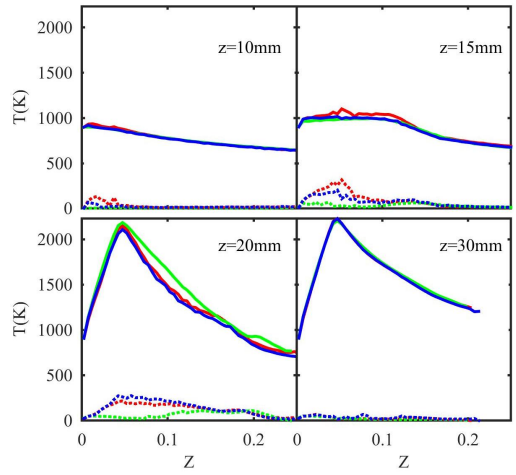

Figure 5: Effect of mixing model on the conditional mean (solid lines) and standard deviation (dotted lines) of temperature at different axial locations. Red line = IEM model, Green = MMC (r_t = 0.935), blue = MMC (r_t = 0.5). The ambient conditions are: ρ_{amb} = 22.8 kg/m^3, T_{amb} = 900 K and $O_{2,amb}$ = 15%.

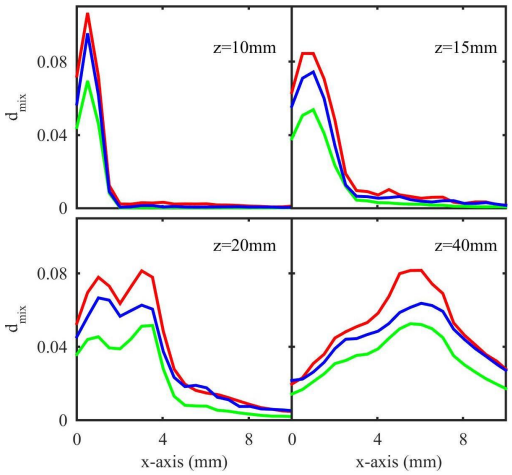

Figure 6: Effect of mixing model on the mixing distance at different axial locations. The legends and the ambient conditions are the same as in Fig. 5.

The choice of the mixing model or of the r_t value for the MMC mixing model do not only influence the FLOL predictions as discussed above, but also have a significant effect on the flame temperature and therefore presumably emission predictions. Figure 5 shows the mean and standard deviation of temperature conditioned on the mixture fraction at four different axial locations for the case with T_{amb} = 900 K and $O_{2,amb}$ = 15%. The location of first-stage ignition is the same for all mixing models and occurs at z = 10 mm. At z = 10 mm (Fig. 5, top-left), there is a minor difference in the conditional mean of the temperature ($\widetilde{T|Z}$) predicted by different mixing models. However, it can be observed that the conditional standard deviation of temperature is higher with the IEM model and the MMC model with r_t = 0.5. The conditional fluctuations from these models are further amplified just upstream of the experimental FLOL (z = 15 mm). The differences in the dissipation of conditional fluctuations exists downstream of the FLOL as well (z = 20 mm). However, there is no significant difference between different mixing models at z = 40 mm, since the flame is in a near equilibrium state with negligible conditional fluctuations.

Finally, Fig. 6 shows the radial profiles of mixing distance at different axial locations. The IEM model has the highest mixing distance since the composition of the notional particles relaxes towards the unconditional mean. In the MMC model, on the other hand, the particles relax towards the mean conditioned on the reference variable, resulting in lower mixing distances between the particles in composition space. The case with r_t = 0.935 (green line) has a lower mixing distance when compared to the one with r_t = 0.5 (blue line) since the composition of the notional particles relaxes at a higher rate towards the conditional mean. A higher r_t value implies higher localness and hence a lower mixing distance in the composition space. These results therefore serve to demonstrate that locality is controllable in the present modelling framework. It should be noted that these trends are independent of the TPDF particle number.

6. Conclusions

RANS-TPDF simulations with IEM and MMC mixing models have been performed for the ECN Spray A cases. The predictions of the mean and standard deviation of mixture fraction were in good agreement with the experimental data for the non-reacting case. The reactive simulations were carried out for different ambient temperature and oxygen conditions. The ignition delay was predicted well by both the IEM and the MMC mixing model. There was a negligible effect of the mixing model on the ignition delay predictions.

The effect of the mixing model on the FLOL predictions was however significant. The IEM model overpredicted the FLOL at high temperature and oxygen conditions. The IEM model predicted consistently a higher FLOL when compared to the MMC model. The MMC model with r_t = 0.935 estimated the FLOL well at all cases except the 800 K case. It was shown that the FLOL is controllable by changing the target correlation

coefficient, while C_ϕ and therefore the mixing fields are held fixed. The mixing model had its most significant impact on the conditional fluctuations of temperature and species mass fraction near the FLOL. The mixing model was further analysed by comparing mixing distances in composition space, and controllable localness was demonstrated.

Further work is needed to establish guidance for setting the parameter r_t, to understand whether and how the optimal value is dependent on conditions and configuration. Extensions of the model to premixed combustion and to other more complicated cases such as multiple injection cases is also envisaged.

Acknowledgments

This work was supported by the Australian Research Council (ARC) under the Discovery Projects funding scheme (DP130100763, DP150104395 and DP150104393). The research benefited from computational resources provided through the National Computational Merit Allocation Scheme, supported by the Australian Government. The computational facilities supporting this project included the Australian NCI National Facility, the partner share of the NCI facility provided by Intersect Australia Pty Ltd., and Pawsey Supercomputing Centre (with funding from the Australian Government and the Government of Western Australia).

References

[1] A. Kronenburg, M. Kostka, Combustion and Flame 143 (2005) 342–356.
[2] R. R. Cao, H. Wang, S. B. Pope, Proceedings of the Combustion Institute 31 (2007) 1543–1550.
[3] Y. Ge, M. J. Cleary, A. Y. Klimenko, Proceedings of the Combustion Institute 34 (2013) 1325–1332.
[4] Z. Luo, S. Som, S. M. Sarathy, M. Plomer, W. J. Pitz, D. E. Longman, T. Lu, Combustion Theory and Modelling 18 (2014) 187–203.
[5] A. Wehrfritz, O. Kaario, V. Vuorinen, B. Somers, Combustion and Flame 167 (2016) 113–131.
[6] S. S. Pandurangi, M. Bolla, Y. M. Wright, K. Boulouchos, S. A. Skeen, J. Manin, L. M. Pickett, International Journal of Engine Research 18 (2017) 436–452.
[7] S. Bhattacharjee, D. C. Haworth, Combustion and Flame 160 (2013) 2083–2102.
[8] Y. Pei, E. R. Hawkes, S. Kook, G. M. Goldin, T. Lu, Combustion and Flame 162 (2015) 2006–2019.
[9] F. Salehi, M. J. Cleary, A. R. Masri, Y. Ge, A. Y. Klimenko, Proceedings of the Combustion Institute 36 (2017) 3577–3585.
[10] S. B. Pope, Progress in Energy and Combustion Science 11 (1985) 119–192.
[11] S. Subramaniam, S. B. Pope, Combustion and Flame 115 (1998) 487–514.
[12] A. Y. Klimenko, Combustion and Flame 143 (2005) 369–385.
[13] C. Dopazo, E. E. O'Brien, Acta Astronautic 1 (1974) 1239–1266.
[14] C. Dopazo, Physics of Fluids 22 (1979) 20.
[15] A. Krisman, J. C. K. Tang, E. R. Hawkes, D. O. Lignell, J. H. Chen, Combustion and Flame 161 (2014) 2085–2106.
[16] A. Y. Klimenko, S. B. Pope, Physics of Fluids 15 (2003) 1907–1925.
[17] A. Varna, M. J. Cleary, E. R. Hawkes, Combustion and Flame 181 (2017) 342–353.
[18] A. Varna, M. J. Cleary, E. R. Hawkes, Combustion and Flame 181 (2017) 354–364.
[19] X. Y. Zhao, D. C. Haworth, Combustion and Flame 161 (2014) 1866–1882.
[20] H. W. Ge, E. Gutheil, Combustion and Flame 153 (2008) 173–185.
[21] A. Varna, M. J. Cleary, E. R. Hawkes, in: 20th Australasian Fluid Mechanics Conference.
[22] S. B. Pope, Turbulent Flows, Cambridge University Press, 2000.
[23] A. P. Wandel, A. Y. Klimenko, Physics of Fluids 17 (2005) 128105.
[24] L. M. Pickett, J. Manin, C. L. Genzale, D. L. Siebers, M. P. B. Musculus, C. A. Idicheria, SAE International Journal of Engines 4 (2011) 764–799.
[25] P. M. Lillo, L. M. Pickett, H. Persson, O. Andersson, S. Kook, SAE Int. J. Engines 5 (2012) 1330–1346.
[26] Engine Combustion Network, Sandia National Laboratories, http://www.sandia.gov/ecn/, 2016.
[27] OpenFOAM, www.openfoam.org, 2017.
[28] M. Muradoglu, S. B. Pope, D. A. Caughey, Journal of Computational Physics 172 (2001) 841–878.
[29] G. D'Errico, T. Lucchini, F. Contino, M. Jangi, X. S. Bai, Combustion Theory and Modelling 18 (2014) 65–88.
[30] N. Nordin, Complex chemistry modeling of diesel spray combustion, Ph.D. thesis, 2001.
[31] T. F. Su, M. A. Patterson, R. D. Reitz, P. V. Farrell, SAE Technical Paper No. 960861 (1996).
[32] T. Lucchini, G. D'Errico, D. Ettorre, International Journal of Heat and Fluid Flow 32 (2011) 285–297.
[33] T. Yao, Y. Pei, B. J. Zhong, S. Som, T. Lu, K. H. Luo, Fuel 191 (2017) 339–349.
[34] W. Jones, B. Launder, International Journal of Heat and Mass Transfer 15 (1972) 301–314.
[35] L. M. Pickett, C. L. Genzale, G. Bruneaux, L. Malbec, L. Hermant, C. Christiansen, J. Schramm, SAE Int. J. Engines 3 (2010) 156–181.
[36] M. Bolla, M. A. Chishty, E. R. Hawkes, S. Kook, International Journal of Engine Research 18 (2017) 6–14.
[37] A. Varna, A. Wehrfritz, E. R. Hawkes, M. J. Cleary, T. Lucchini, G. DErrico, in: 11th Asia-Pacific Conference on Combustion.
[38] A. Maghbouli, T. Lucchini, G. D'Errico, A. Onorati, L.-M. Malbec, M. Musculus, W. Eagle, SAE Technical Paper No. 2016-01-0577 (2016).
[39] M. A. Chishty, Y. Pei, E. R. Hawkes, M. Bolla, S. Kook, in: 19th Australasian Fluid Mechanics Conference, December, pp. 19–22.
[40] Y. Pei, E. R. Hawkes, S. Kook, Flow, Turbulence and Combustion 91 (2013) 249–280.